NASA
Technical
Paper
2461

May 1985

# Performance and Surge Limits of a TF30-P-3 Turbofan Engine/Axisymmetric Mixed-Compression Inlet Propulsion System at Mach 2.5

Joseph F. Wasserbauer,
Harvey E. Neumann,
and Robert J. Shaw

NASA

**NASA Technical Paper 2461**

1985

# Performance and Surge Limits of a TF30-P-3 Turbofan Engine/Axisymmetric Mixed-Compression Inlet Propulsion System at Mach 2.5

Joseph F. Wasserbauer,
Harvey E. Neumann,
and Robert J. Shaw

*Lewis Research Center*
*Cleveland, Ohio*

NASA
National Aeronautics
and Space Administration

**Scientific and Technical Information Branch**

## Summary

Steady-state performance, integrated control system techniques, and inlet-engine compatibility were investigated with a low-bleed inlet. The inlet had minimum internal contraction, consistent with high total pressure recovery and low cowl drag. The inlet-engine combination displayed good performance with only about 2 percent of inlet performance bleed. At the match inlet-engine operating condition the inlet pressure recovery was 0.895 at a diffuser throat-exit mass flow ratio of 0.977. The inlet-engine combination had large-angle-of-attack capability with about 6 percent performance bleed. Angle of attack was limited to 5.58° by engine surge. The turbofan engine displayed a high tolerance to the generated inlet distortion.


## Introduction

Supersonic inlets should operate efficiently with low drag over the entire flight range of the aircraft. For flight speeds above Mach 2.0, mixed-compression inlets offer this capability. Proper operation and control of the propulsion system requires a knowledge of the steady-state and dynamic interactions between the inlet and the engine. Operation and control of a mixed-compression inlet coupled to a turbojet engine have been investigated (refs. 1 to 4). However, considerable interest exists in the use of turbofan engines coupled to mixed-compression inlets as propulsion systems for future supersonic transport aircraft. Therefore the low-bleed, mixed-compression axisymmetric inlet of reference 5 coupled to a TF30-P-3 turbofan engine, was tested in the Lewis 10- by 10-Foot Supersonic Wind Tunnel.

The objectives were (1) to determine the overall steady-state performance of the mixed-compression inlet-turbofan engine combination, (2) to study the interactions of such a system and determine its controllability, and (3) to determine the amplitude and spatial distribution of the steady-state and dynamic distortions produced in the inlet and the effects of these distortions on the engine surge limits. The dynamic interaction and controllability of this inlet-engine combination have been reported in references 6 to 8. Some steady-state and dynamic distortion results are presented in references 9 and 10. The present report gives the overall steady-state performance and surge limits of the cold-pipe inlet of reference 5 coupled to the TF30-P-3 turbofan engine.

The inlet-engine combination was tested at a free-stream Mach number of 2.5. Flow surveys were made at the compressor face and throughout the turbofan engine. Both steady-state and dynamic instrumentation were used to record the total pressures at the compressor face. Steady-state and root-mean-square data are presented in this report. Steady-state data representing inlet and engine operating parameters are presented for inlet-engine operation at zero and positive angles of attack. Engine surge limits with distortion are presented for operation at positive angles of attack and at extremely supercritical terminal shock positions.

## Symbols

| | |
|---|---|
| $A_j$ | exhaust nozzle area, percent of rated area |
| $H$ | annulus height, m |
| $h$ | distance from centerbody surface, m |
| $K_{d2}$ | circumferential distortion index (defined in appendix) |
| $K_{ra}$ | radial distortion index (defined in appendix) |
| $m/m_0$ | mass flow ratio |
| $N_1$ | low-pressure-compressor mechanical rotor speed, rpm |
| $N_2$ | high-pressure-compressor mechanical rotor speed, rpm |
| $P$ | total pressure |
| $\Delta P$ | fluctuating component of total pressure |
| $R_c$ | cowl lip radius (0.4745 m) |
| RNI | Reynolds number index, $\delta/\varphi \sqrt{\theta}$ |
| $T$ | temperature, °R |
| $W_{ac}$ | core compressor airflow, kg/sec |
| $W_{at}$ | total airflow, kg/s |
| $x$ | axial location, m |
| $\delta$ | $P/P_{sl}$ |
| $\theta$ | $T/T_{sl}$ |
| $\mu$ | absolute viscosity, kg s/cm |

| | |
|---|---|
| $\varphi$ | $\mu/\mu_{sl}$ |

Subscripts:

| | |
|---|---|
| av | average |
| by | bypass |
| $f$ | fan |
| max | maximum |
| min | minimum |
| rms | root mean square |
| sl | standard sea-level conditions |
| 0 | free stream |
| 2,2.3, 3, etc. | station locations (fig. 5) |

## Apparatus and Procedure

The axisymmetric inlet (figs. 1 and 2) had 45-percent internal compression and a translating centerbody with half-cone angles of 12.5° and 18.5° for the first and second cones, respectively. This design concept was used

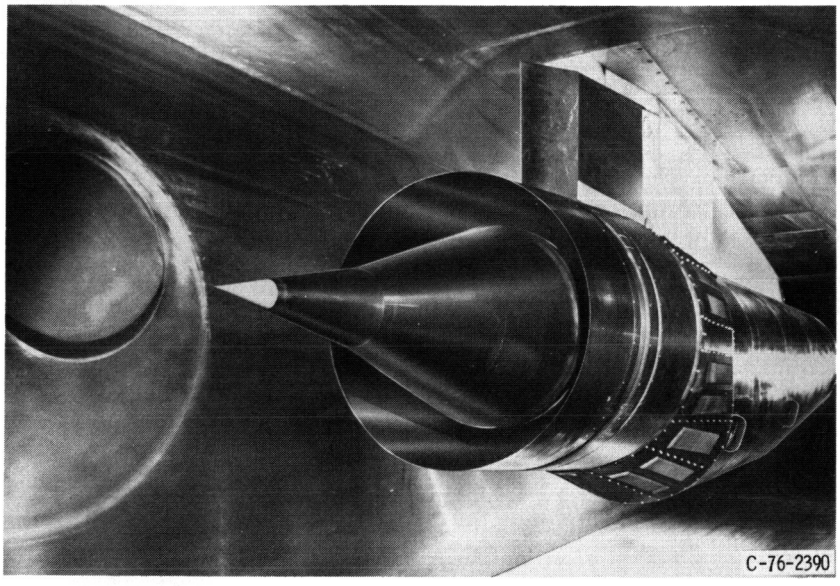


Figure 1.—TF30-P-3 model installed in 10- by 10-Foot Supersonic Wind Tunnel.

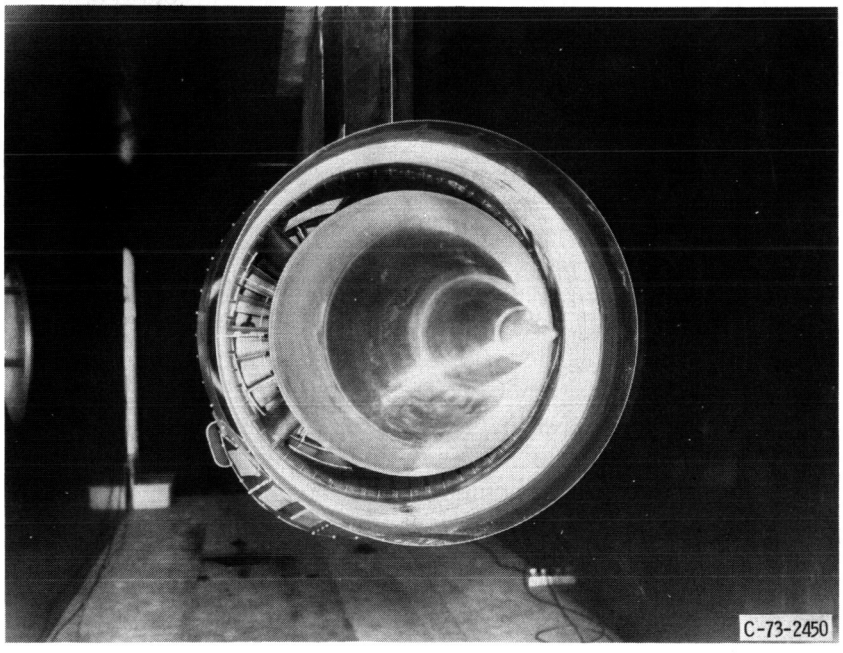


Figure 2.—Head-on view of model showing TF30-P-3 fan.

to provide the maximum external compression compatible with high total pressure recovery and relatively low cowl drag. The focusing concept of this inlet permitted significant shortening of the supersonic diffuser (from cowl lip to inlet throat) and thus reduced the amount of cowl bleed necessary at the throat. To vary the contraction ratio for a flight inlet, the second cone would be collapsed, and at its lowest position it would blend into the first-cone contours so as to provide a single-cone centerbody. This concept is known as the variable diameter centerbody (VDC) inlet. For wind tunnel testing the translating centerbody feature was used for inlet restarts. Fifty-five percent of the inlet's supersonic area contraction occurred externally and 45 percent internally at the design Mach number of 2.5. The inlet was sized to provide the airflow demand of the turbofan engine at Mach 2.5. The inlet had a capture area of 0.707 $m^2$ and measured 1.80 m from the cowl lip to the fan face. The inlet design and performance are described in reference 5.

Boundary layer bleed on the centerbody was provided by locating a flush slot at the shoulder of the inlet throat. The centerbody bleed flow was ducted to four equally spaced hollow centerbody support struts located in the diffuser section (fig. 3). Centerbody bleed flow was controlled by a butterfly valve in each strut. The butterfly valves were positioned by electrohydraulic servos with rotary hydraulic actuators. Cowl bleed was not necessary for high-performance stable inlet operation.

The inlet was also equipped with eight slotted-plate overboard bypass doors to match inlet-engine airflow (fig. 3). To evaluate inlet dynamics and inlet control

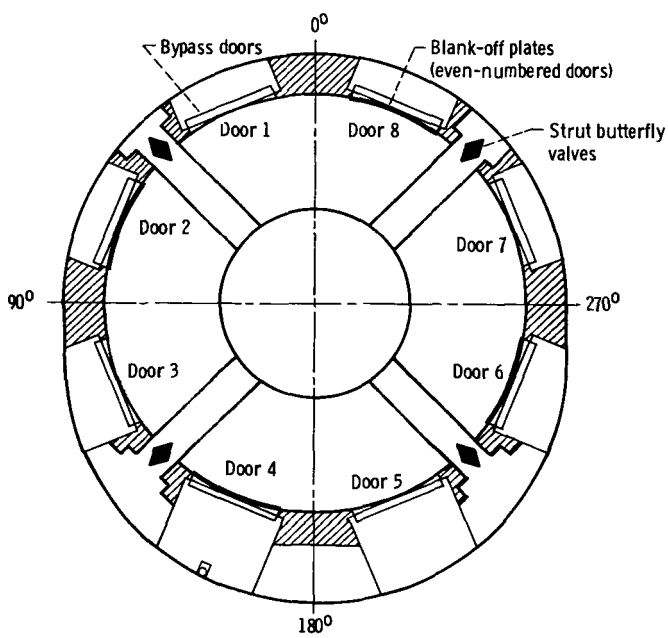


Figure 3.—View of inlet looking downstream, showing bypass doors and centerbody bleed flow struts.

concepts, the even-numbered doors were oscillated to create a flow disturbance; the odd-numbered doors were used to counteract this disturbance during the dynamic testing (ref. 7). The disturbance doors (even numbered) had 87.5 percent of their exit area blocked with blank-off plates. The total geometric flow area of the four control doors (odd numbered) was 0.161 $m^2$, and that of the four disturbance doors was 0.0200 $m^2$. The blank-off plates were not removed during this test. Figure 4 shows the full bypass entrance for a control door and the single bypass slot entrance of a blanked-off disturbance door, as well as some of the compressor-face rake instrumentation.

The engine used in this investigation was a Pratt & Whitney TF30-P-3. The TF30-P-3 is an axial, mixed-flow, augmented, twin-spool, low-bypass-ratio turbofan engine with a variable-area convergent primary nozzle. The inlet-engine combination is shown schematically in figure 5, with the engine stations designated. A three-stage, axial-flow fan is mounted on the same shaft with a six-stage, axial-flow, low-pressure compressor. This unit is driven by a three-stage, low-pressure turbine. A seven-stage, axial-flow compressor driven by a single-stage, air-cooled, turbine makes up the high-pressure spool. The compressor is equipped with seventh-stage (low-pressure compressor) and twelfth-stage (high-pressure compressor) bleeds. The seventh-stage bleed is normally operated by the aircraft control system; the twelfth-stage bleed is normally operated by the engine control system. For these tests the seventh- and twelfth-stage bleeds were operated manually and the engine afterburner was not used.

The engine surge data reported herein were for an exhaust nozzle area set for 100 percent of rated. The engine surge points are of the "drift stall" type. The procedure was to determine the value of the variable parameter (engine speed, bypass door setting, or inlet angle of attack) at surge. The point was then repeated with a slightly conservative value for the variable parameter. If surge did not occur within 3 min, the point was repeated with a variable parameter value closer to the one that caused surge during the search. The test procedure attempted to cover the inlet conditions that produce surge by causing steady-state and dynamic total pressure distortions at the fan face. Three operating conditions were examined:

(1) The engine was set at a constant corrected speed and 100-percent exhaust nozzle area. The overboard bypass doors were positioned to create a supercritical inlet condition (diffuser terminal shock downstream of the inlet throat). The increased dynamic distortion (due to a greater shock-boundary layer reaction) combined with steady-state distortion to induce surge.

(2) The engine speed was increased at a low bypass door setting and 100-percent exhaust nozzle area, to create a supercritical inlet condition. Again the resultant rise in dynamic distortion combined with the correspondingly greater steady-state distortion to induce surge.

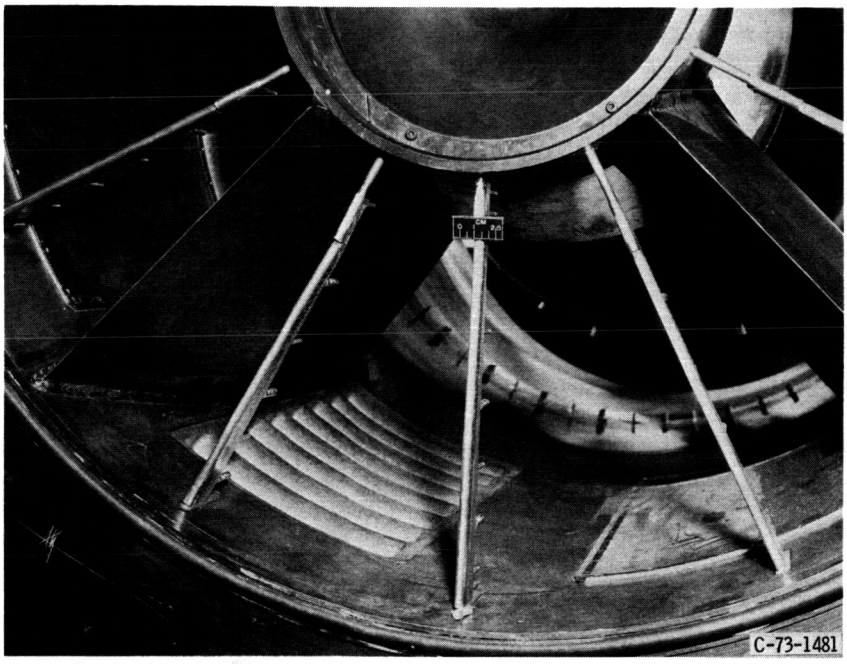


Figure 4.—Bypass entrance (odd-numbered door) and partial blanked-off bypass entrance (even-numbered door), looking upstream from diffuser exit.

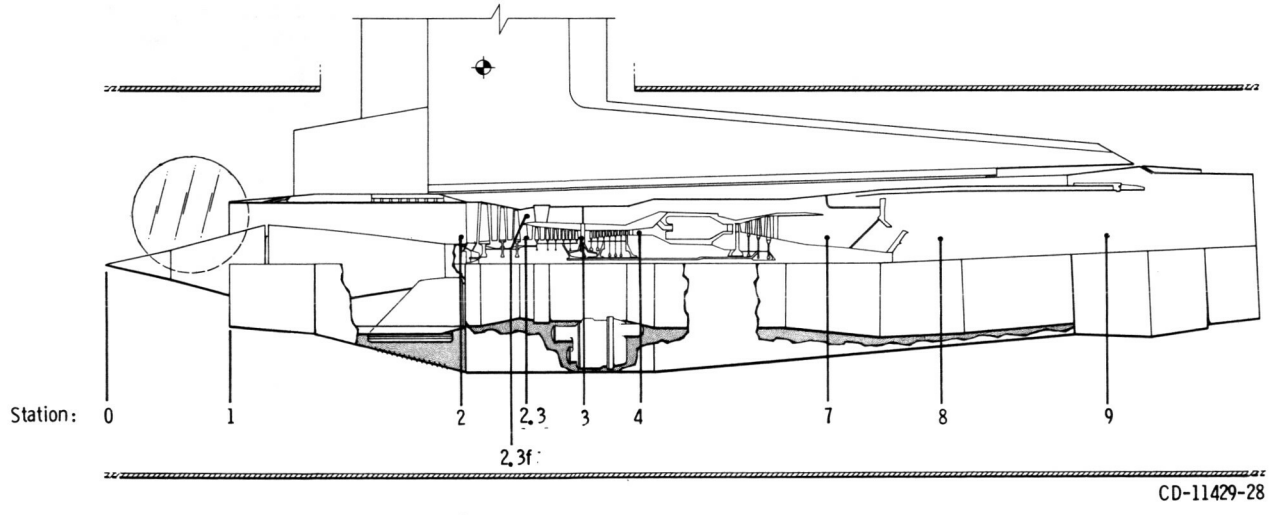


Figure 5.—Cross section of inlet and TF30-P-3 installed in 10- by 10-Foot Supersonic Wind Tunnel, showing inlet-engine stations and instrumentation locations.

(3) The engine was set at a constant corrected speed and 100-percent exhaust nozzle area. At a selected bypass door exit area the inlet angle of attack was set at a preselected value. The bypass door exit area was then increased until the combined dynamic and steady-state distortion induced engine surge.

## Instrumentation

The instrumentation locations in the propulsion system are shown in figure 5. Details of instrumentation at each propulsion system station, starting with station 2, are illustrated in figure 6. The fan-face instrumentation at station 2 (fig. 6(a)) was used to describe the flow characteristics at the inlet-engine interface. The overall total pressure recovery and distortion parameters were determined by using pressures from rakes 1 to 12, which had six area-weighted tubes per rake. Rakes 1, 7, and 10 had three additional total pressure probes to better define the boundary layer on the cowl and centerbody at the diffuser exit. The angular location of the 12 rakes had been adjusted for the presence of the four struts. This

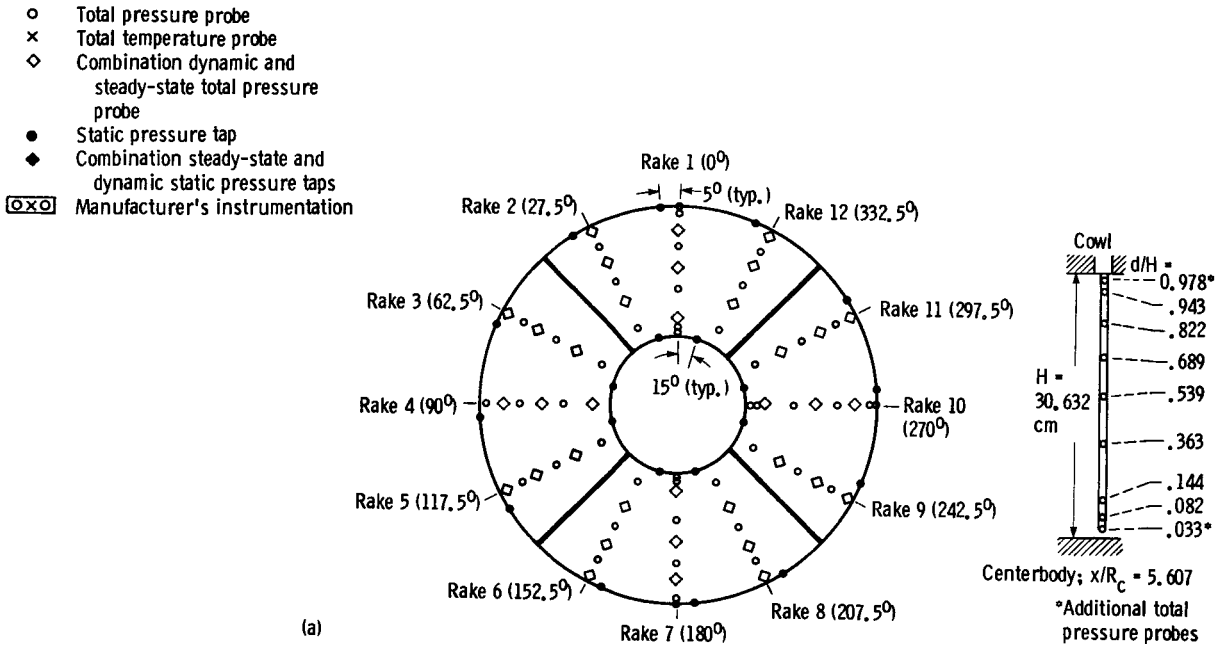


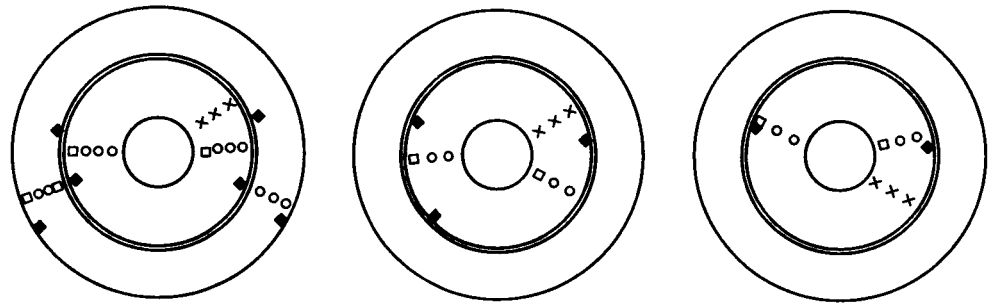

Stations 2.3 and 2.3f: fan discharge and low-pressure-compressor inlet

Station 3: low-pressure-compressor discharge; high-pressure-compressor inlet

Station 4: high-pressure-compressor discharge

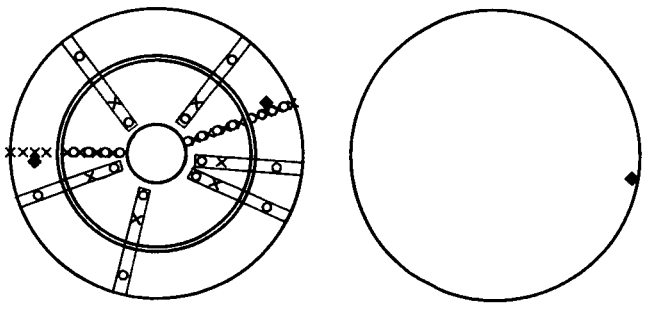

Station 7: turbine discharge

Stations 8 and 9: afterburner can

(b)

(a) Diffuser exit steady-state and dynamic pressure instrumentation, at station 2, looking downstream.
(b) Engine steady-state and dynamic pressure instrumentation, looking downstream.

Figure 6.—Detailed instrumentation.

resulted in a 2.5° correction on 8 of the 12 rakes adjacent to the struts. Rakes 12, 3, 6, and 9 were positioned downstream of the blanked-off bypass doors. Wall static pressure was measured with 20 taps.

To measure the fluctuating component of total pressure, subminiature absolute pressure transducers were mounted in the rakes at 36 locations (fig. 6a)). The transducers were mounted such that steady-state and dynamic pressure could be measured simultaneously. The resultant configuration provided a flat response to at least 1000 Hz. The fluctuating component of the signal was passed through a second-order, low-pass filter with a 1000-Hz corner frequency and was measured with a true rms meter. At each steady-state operating condition the average value of these rms measurements was ratioed to the average steady-state total pressure recovery. This parameter is defined herein as the dynamic distortion for that particular operating condition. The filtered fluctuating component of each pressure transducer was also recorded on frequency-modulated magnetic tape.

Steady-state static and total pressures were measured in the engine at stations 2.3, 2.3f, 3, 4, and 7 (fig. 6(b)). Only static pressures were measured at stations 8 and 9. Dynamic static and total pressures were measured at stations 2.3, 2.3f, 3, 4, 8, and 9. Only total temperatures were measured at stations 2.3, 3, 4, and 7. The manufacturer's instrumentation is also shown at station 7. Although the output from all of this engine instrumentation is not given herein, the instrumentation is included at this point for completeness.

All data were recorded at the following average free-stream conditions: Mach number, 2.5; total temperature, 297 K; total pressure, 9.3 N/cm$^2$; unit Reynolds number, 8.2 million per meter; and specific-heat ratio, 1.4.

## Results and Discussion

The results reported herein are presented in two parts: first, the steady-state, inlet-engine operating performance at zero angle of attack; second, the data for engine surges at zero and positive angles of attack for both design engine and supercritical inlet operation.

### Inlet-Engine Performance

The compressor maps for the turbofan engine shown in figure 7 were experimentally determined in the study presented in reference 11. Each map shows component pressure ratio versus percent of corrected airflow for military operation at a 0.50 RNI, as well as the engine operating line for the design nozzle exit area ($A_j = 100$ percent of rated) and the engine speed lines as percent of rated military speed. The rated military core flow, corrected to station 3, was 12.9 kg/s. The rated sea-level static military total flow, corrected to fan-face conditions, was 107 kg/s. The rated military corrected speeds for the low- and high-pressure compressors were 9525 and 10 360 rpm, respectively. Because of insufficient instrumentation in the fan duct and compressor core, experimental values of the bypass flows were not accurately known. The pressure ratio and corrected speed were therefore used to indicate experimental performance on the core compressor maps. The fan performance was determined by the corrected airflow at the diffuser exit (fan face) and the pressure ratio.

At Mach 2.5 the corrected airflow required for the turbofan engine was 62 percent of the rated sea-level static military value and the corrected engine speed about 65 percent. The engine speed would be nearly 100 percent of the rated mechanical speed. However, the tunnel free-stream total temperature did not match the true flight conditions. Therefore the engine speed was reduced so that, with the nozzle area set at 100 percent of the military rated area, Mach 2.5 operation was simulated with the proper corrected speed and corrected airflow.

The experimental data were obtained at 65 percent of the corrected military airflow, or at a selected match corrected airflow of about 68.49 kg/s. This was higher than the 65.77-kg/s design airflow and allowed the engine to operate at higher mechanical speeds. Because the inlet performance bleed was low, additional inlet bypass flow was needed to match the selected engine corrected airflow requirements. The bypass mass flow ratio was 0.035 for the selected match corrected airflow of 68.49 kg/s. If the design corrected airflow of 65.77 kg/s were used, about twice as much bypass mass flow ratio would have been required.

The experimental data presented in figure 7 show the range of the engine operation for this test. The tailed symbols indicate engine operation at selected inlet-engine match corrected airflow. For these operating conditions the engine mass flow ratio and pressure recovery at the fan face were varied by spilling inlet mass flow through the inlet bypass system while maintaining constant engine speed. Engine speed variation is identified by the untailed symbols. Here, the fan-face corrected airflow was increased from the selected match inlet-engine operating condition by maintaining constant engine mass flow ratio and reducing the fan-face pressure recovery. The pressure recovery was reduced by relocating the inlet terminal shock in the subsonic diffuser downstream of the inlet throat. This is called supercritical inlet operation.

At a free-stream Mach number of 2.5 with the operating turbofan engine (fig. 8; table I) the same values of pressure recovery were obtained as were recorded during the cold-flow tests of reference 5. The peak inlet pressure recovery was 0.895 (inlet-engine selected match point) with a performance bleed mass flow ratio of only 0.019. Since the inlet was designed to spill a small amount of mass flow at cruise, the diffuser throat-exit mass flow ratio was 0.977. The inlet-engine selected match

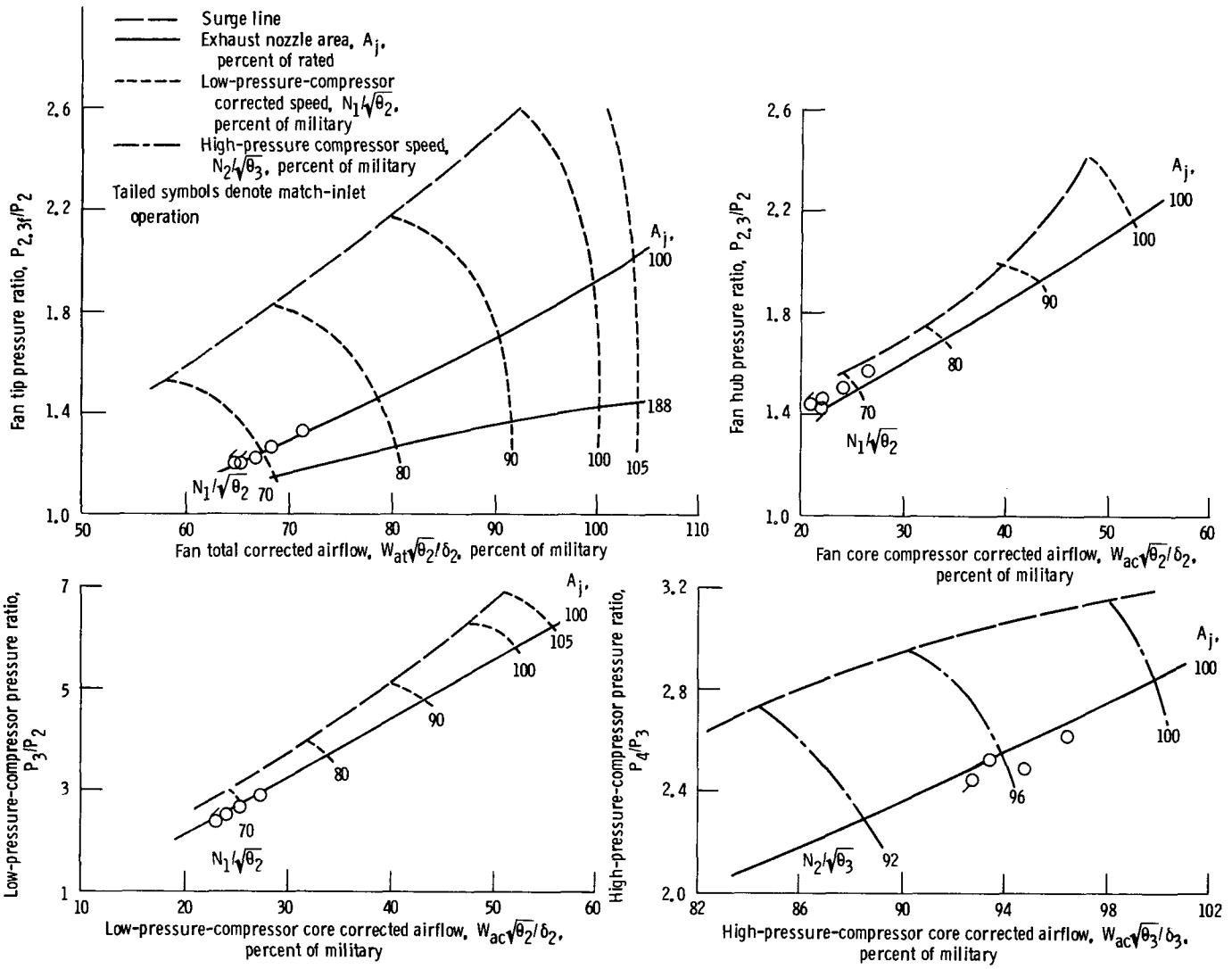


Figure 7.—Compressor performance. (Tailed symbols denote match inlet-engine operation.)

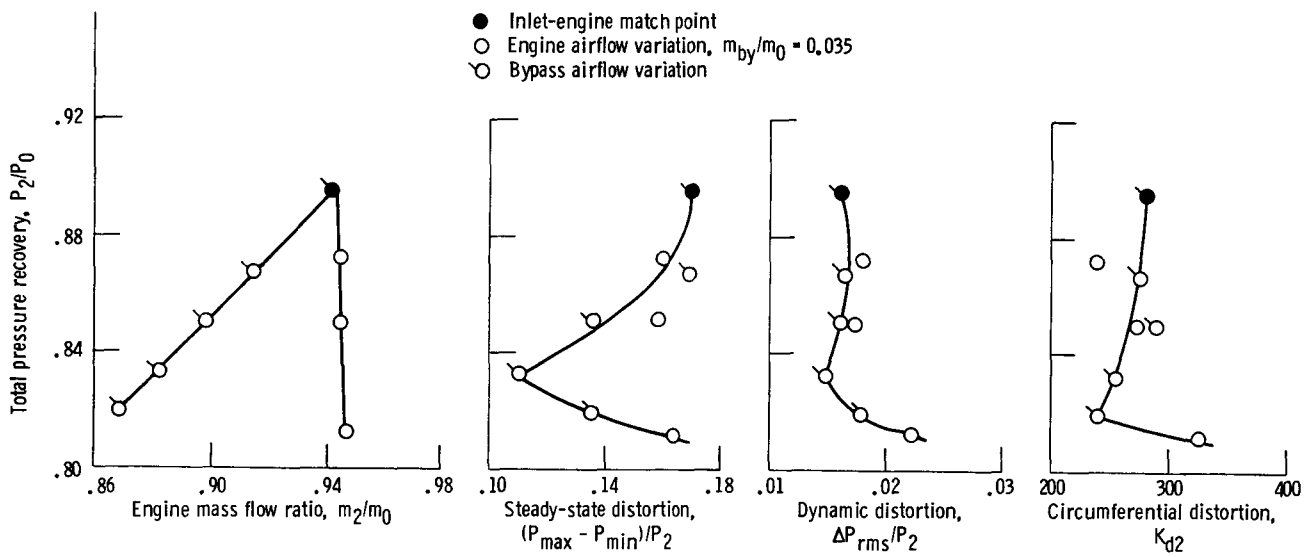


Figure 8.—Inlet performance at Mach 2.5.

TABLE I.—INLET-ENGINE PERFORMANCE DATA AT ZERO ANGLE OF ATTACK

| Engine mass flow ratio, $m_2/m_0$ | Total pressure recovery, $P_2/P_0$ | Steady-state distortion, $\frac{P_{max}-P_{min}}{P_2}$ | Dynamic distortion, $\Delta P_{rms}/P_0$ | Circumferential distortion index, $K_{d2}$ | Engine corrected airflow, $W\sqrt{\theta_2}/\delta_2$ | Low-pressure compressor corrected speed, $N_1/\sqrt{\theta_2}$ | High-pressure compressor corrected speed, $N_2/\sqrt{\theta_3}$ | Fan pressure ratio, $P_{2.3f}/P_2$ | Fan core pressure ratio, $P_{2.3}/P_2$ | Low-pressure-compressor pressure ratio, $P_3/P_2$ | High-pressure-compressor pressure ratio, $P_4/P_3$ |
|---|---|---|---|---|---|---|---|---|---|---|---|
| 0.942 | 0.895 | 0.170 | 0.016 | 280.5 | 151.4 | 6235.3 | 9 822.4 | 1.209 | 1.453 | 2.449 | 2.449 |
| .915 | .867 | .169 | .016 | 278.9 | 151.0 | 6259.0 | 9 822.8 | 1.208 | 1.451 | 2.457 | 2.445 |
| .899 | .851 | .136 | .016 | 289.3 | 151.1 | 6293.4 | 9 809.7 | 1.207 | 1.450 | 2.463 | 2.442 |
| .882 | .834 | .110 | .015 | 256.0 | 151.4 | 6245.3 | 9 817.8 | 1.205 | 1.452 | 2.454 | 2.449 |
| .869 | .820 | .136 | .018 | 240.3 | 151.7 | 6221.3 | 9 816.1 | 1.206 | 1.455 | 2.447 | 2.453 |
| .944 | .850 | .159 | .017 | 274.3 | 158.9 | 6582.1 | 9 942.4 | 1.264 | 1.508 | 2.671 | 2.523 |
| .947 | .813 | .163 | .022 | 325.6 | 166.7 | 6847.1 | 10 082.0 | 1.332 | 1.582 | 2.903 | 2.608 |
| .944 | .872 | .160 | .018 | 240.8 | 154.9 | 6357.0 | 9 969.2 | 1.226 | 1.474 | 2.507 | 2.483 |

condition was obtained by bypassing 0.035 of the inlet's capture mass flow ratio so that the engine mass flow ratio was 0.942. Dynamic distortion varied from 0.015 to 0.022 over the range of inlet conditions. Even at the "far supercritical" inlet operating conditions the dynamic activity was within acceptable limits, with a value of 0.022. Reference 5 shows slightly higher values for dynamic distortion (0.0175 to 0.025) than are shown herein. However, in that study only three probes were used to obtain the average dynamic activity as compared with 36 in this test.

The circumferential distortion index $K_{d2}$ varied from 240 to 325 (fig. 8). All distortion values were lower than those necessary to cause surge. Steady-state distortion values should be correspondingly low, especially at and near the match inlet-engine operating condition. However, the steady-state distortion of 0.17 at the match point was about 25 percent larger than expected from data recorded in reference 5.

The total pressure profiles for each rake at the match inlet-engine operating condition (fig. 9(a)) do not show excessive distortion except for rake 12. Here flow separation at the cowl surface is evident and the flow profile is highly distorted. The flow profiles of rakes 1 and 2, which were in the same quadrant as rake 12, appear to be good. Rake 12, however, measures the flow just downstream of the blank-off plate for the bypass door, about 2.5 cm from the edge of the plate. Protrusion of the plate into the duct stream (about 0.32 cm) at this point in the duct could have induced flow separation. However, rakes 3, 6, and 9 also measured flow behind blank-off plates and show acceptable profiles with no separation. After a thorough check of the rake data no reason could be found to question the pressure values of rake 12. This therefore appears to be a localized phenomena with an unknown cause. Eliminating the flow separation at rake 12 would have resulted in a steady-state distortion value of 0.10 at the match condition. In reference 5 the distortion at that condition was about 0.10 when the bypass doors were sealed and about 0.12 when the bypass doors were operating. The total pressure profiles for a supercritical operating condition (bypass doors open) at the match corrected airflow (fig. 9(b)) again show flow separation at rake 12. The steady-state distortion would have been 0.095 if the separation had not occurred.

## Inlet-Engine Compatibility

All surge events obtained in this investigation were of the "drift stall" type. That is, after equilibrium operation of the propulsion system was established at an incipient stalling condition, an engine surge occurred because of some random dynamic flow perturbation within the inlet. The set of surge events recorded as part of this program have been analyzed and reported in references 9 and 10. The surges were generally preceded by a rotating stall, appearing first in either the fan or the low-pressure compressor. Approximately one rotor revolution after the first appearance of the rotating stall a surge wave emanated from the high-pressure compressor.

The performance of the compressor at the incipient surge operating condition is tabulated in table II. The engine compressor maps and the experimental performance data for incipient surge operation are shown in figure 10. The maps (from ref. 9) are those previously presented in figure 7. The fan tip and the high-pressure compressor performed near their undistorted operating lines. The fan hub and the low-pressure compressor showed considerable scatter about their normal operating lines. Data below the operating lines of the fan hub and the low-pressure compressor are for zero angle of attack with the inlet operating supercritically. The compressor experienced a four-per-revolution distortion pattern with a strong radial component when operating at these conditions, as discussed later in this section.

The data above the operating lines of the fan hub and the low-pressure compressor were for angle-of-attack operation. The available stall margin was therefore smaller for angle-of-attack operation than for the severe supercritical operation at zero angle of attack. For angle-

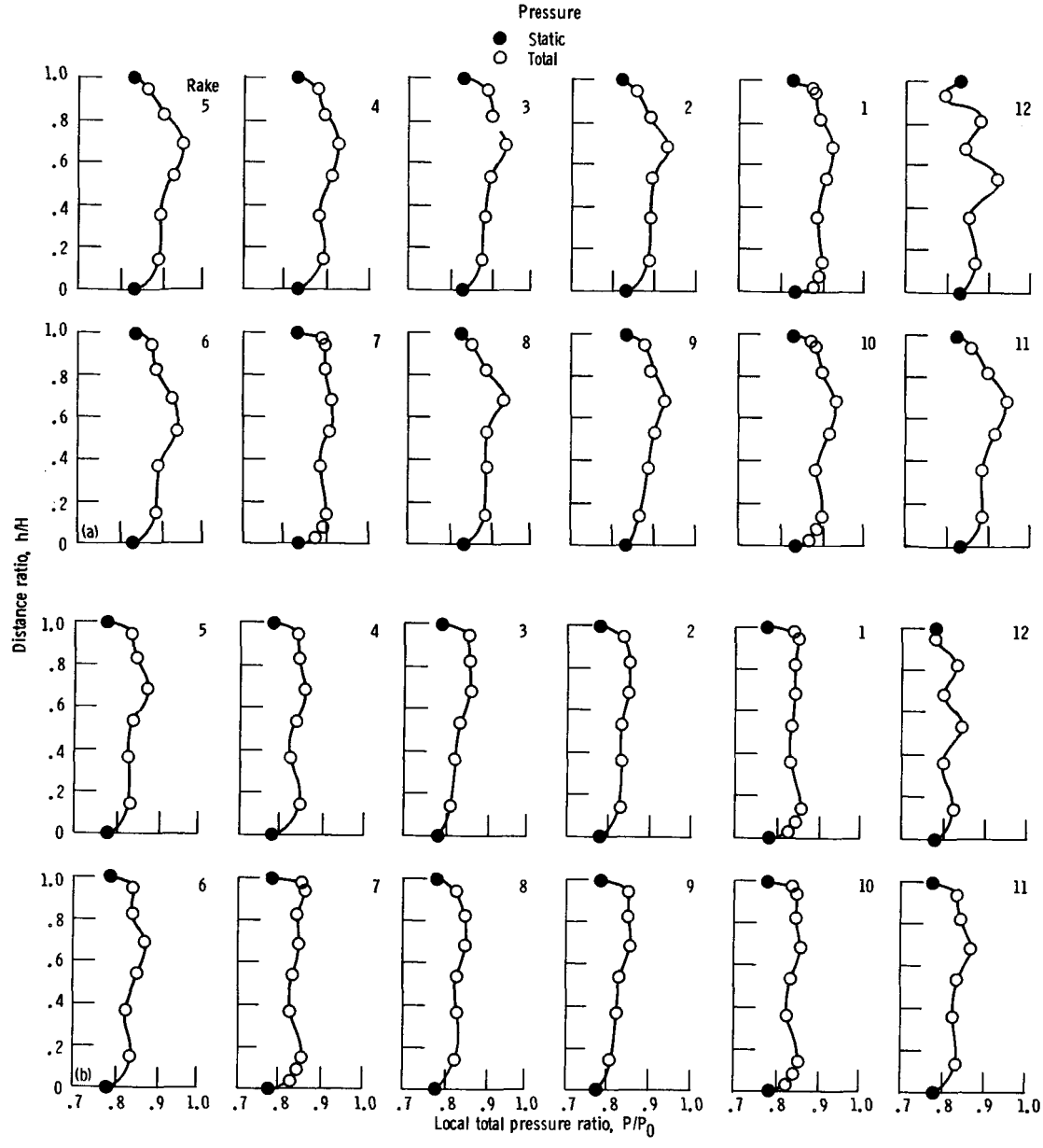


(a) Match inlet-engine operating condition.
(b) Supercritical operating condition.

Figure 9.—Radial total pressure profiles at compressor face.

of-attack operation the distortion was more closely categorized as one-per-revolution circumferential. Inasmuch as the TF30-P-3 is more sensitive to one-per-revolution circumferential distortions than to multiple-per-revolution, or radial, distortions, the compressor can sustain a larger loss in stall margin for zero angle of attack with the inlet operating supercritically than for angle-of-attack operation.

The surge data presented in table II were also studied in reference 10, where surge was classified according to the order of the events leading up to it. With the twelfth-stage bleed closed and the inlet operating in a severe supercritical mode at zero angle of attack, the surge wave emanating from the high-pressure compressor was preceded by rotating stall in the low-pressure compressor. With the twelfth-stage bleed open the initial instability was the surge wave in the high-pressure compressor.

When the inlet-engine system was operated at positive angles of attack, slight changes in operating conditions significantly altered the order of events leading to surge but had little effect on performance. For example, inlet-engine performance was similar at 2.88° and 3.04° angle of attack. A 2.88° rotating stall was detected first in the low-pressure compressor and then in the high-pressure

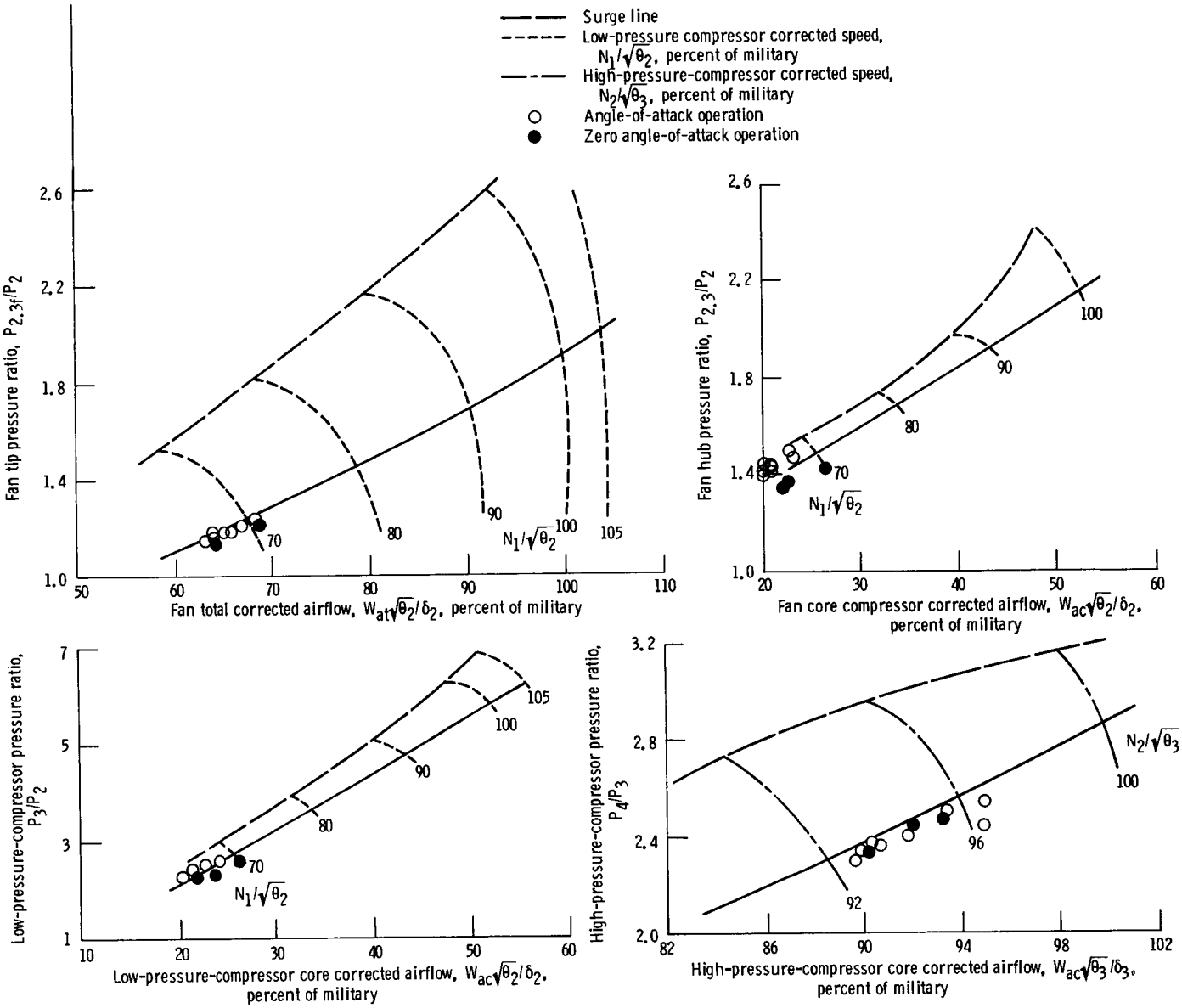


Figure 10.—Compressor performance during incipient surge operation at angle of attack.

compressor. The breakdown in the flow resulted from the surge wave in the high-pressure compressor. At 3.04° the sequence did not include stall in the high-pressure compressor.

Angle-of-attack inlet performance at a free-stream Mach number of 2.5 with the operating turbofan engine at incipient surge is shown in figure 11. The solid lines denote operation at zero angle of attack (fig. 8). The seventh-stage bleed had a stabilizing effect on propulsion system operation. Opening the bleed permitted more extremely supercritical operation. As a result the system could operate at lower recoveries and higher steady-state and dynamic distortions with the seventh-stage bleed open than with it closed.

At zero angle of attack the incipient surge condition was obtained by operating the inlet at extremely supercritical shock positions. As a result the recoveries at surge were generally extremely low (table II) and were associated with larger overboard bypass flows. Extracting these relatively large overboard bypass flows through the four unblocked flow passages resulted in an asymmetric flow configuration. The flow was further distorted by the secondary flows associated with the four large struts within the diffusing section of the inlet. The resultant steady-state distortions were primarily radial with a severe superimposed four-per-revolution distortion. Angle-of-attack operation of the propulsion system generally added a one-per-revolution pressure distortion.

TABLE II.—INLET-ENGINE SURGE DATA

| Engine corrected airflow, $W\sqrt{\theta_2/\delta_2}$ | Engine mass flow ratio, $m_2/m_0$ | Total pressure recovery, $P_2/P_0$ | Angle of attack, deg | Steady-state distortion, $\frac{P_{max}-P_{min}}{P_2}$ | Dynamic distortion, $\Delta P_{rms}/P_0$ | Circumferential distortion index, $K_{d2}$ | Radial distortion index, $K_{rs}$ | Low-pressure compressor corrected speed, $N_1/\sqrt{\theta_2}$ | High-pressure compressor corrected speed, $N_2/\sqrt{\theta_3}$ | Fan pressure ratio, $P_{2.3}/P_2$ | Fan core pressure ratio, $P_{2.3}/P_2$ | Low-pressure-compressor pressure ratio, $P_3/P_2$ | High-pressure-compressor pressure ratio, $P_4/P_3$ |
|---|---|---|---|---|---|---|---|---|---|---|---|---|---|
| Engine bleeds: 7th open, 12th closed | | | | | | | | | | | | | |
| 148.7 | 0.707 | 0.681 | 0 | 0.324 | 0.072 | 412 | 0.484 | 6147 | 9626 | 1.140 | 1.355 | 2.281 | 2.320 |
| 148.6 | .705 | .679 | ↓ | .325 | .073 | 423 | .486 | 6149 | 9621 | 1.140 | 1.356 | 2.283 | 2.318 |
| 148.6 | .707 | .680 | | .325 | .072 | 403 | .476 | 6143 | 9626 | 1.139 | 1.355 | 2.281 | 2.318 |
| 159.7 | .768 | .688 | | .315 | .074 | 391 | .488 | 6660 | 9880 | 1.227 | 1.431 | 2.585 | 2.471 |
| 149.4 | .807 | .773 | 2.37 | .284 | .034 | 871 | .026 | 6004 | 9672 | 1.160 | 1.428 | 2.292 | 2.377 |
| 159.0 | .853 | .768 | 2.36 | .267 | .038 | 855 | .085 | 6455 | 9900 | 1.241 | 1.504 | 2.572 | 2.506 |
| 150.1 | .886 | .845 | 5.58 | .263 | .024 | 1252 | .047 | 6007 | 9760 | 1.166 | 1.423 | 2.261 | 2.402 |
| 159.9 | .905 | .810 | 2.88 | .200 | .027 | 671 | .035 | 6502 | 9994 | 1.254 | 1.507 | 2.600 | 2.543 |
| 159.4 | .904 | .812 | 3.04 | .210 | .027 | 829 | .029 | 6487 | 9984 | 1.247 | 1.505 | 2.586 | 2.539 |
| 153.0 | .827 | .774 | 1.56 | .268 | .039 | 803 | .131 | 6221 | 9800 | 1.191 | 1.459 | 2.410 | 2.435 |
| Engine bleeds: 7th closed, 12th closed | | | | | | | | | | | | | |
| 148.5 | 0.898 | 0.866 | 3.78 | 0.195 | 0.020 | 815 | 0.048 | 6011 | 9604 | 1.156 | 1.430 | 2.382 | 2.296 |
| 145.8 | .872 | .856 | 2.24 | .178 | .022 | 579 | .150 | 6031 | 9607 | 1.150 | 1.415 | 2.368 | 2.291 |
| 155.1 | .902 | .833 | 1.91 | .127 | .020 | 404 | .253 | 6465 | 9768 | 1.214 | 1.477 | 2.641 | 2.400 |
| 150.9 | .887 | .841 | 2.00 | .199 | .023 | 817 | .064 | 6223 | 9687 | 1.187 | 1.458 | 2.509 | 2.352 |
| 149.0 | .838 | .805 | 0 | .196 | .026 | 704 | .045 | 6144 | 9648 | 1.166 | 1.448 | 2.458 | 2.330 |
| 149.4 | .827 | .793 | 1.55 | .233 | .032 | 790 | .043 | 6148 | 9624 | 1.180 | 1.450 | 2.466 | 2.346 |
| Engine bleeds: 7th open, 12th open | | | | | | | | | | | | | |
| 147.9 | 0.692 | 0.670 | 0 | 0.371 | 0.078 | 443 | 0.535 | 6345 | 9989 | 1.182 | 1.370 | 2.293 | 2.418 |

The gradients in total pressure associated with these composite distortions caused higher steady-state distortion (fig. 11). Steady-state distortions in terms of $(P_{max}-P_{min})/P_2$ were two to three times greater at positive angles of attack than at zero angle of attack.

The larger spatial gradients in total pressure associated with angle-of-attack operation increased the turbulence at the compressor face (fig. 11) by about 1 percent of the compressor-face total pressure. When the seventh-stage engine bleed was open, the engine in general could tolerate larger distortions. As a result at incipient surge the inlet operated at a more extremely supercritical shock position and higher distortion with the seventh-stage bleed open.

For supercritical incipient-surge operation at zero angle of attack (fig. 12(a)), the four-per-revolution pattern associated with secondary flow resulted in low-pressure regions in the central segments of each flow passage formed by the struts. The high-pressure region near the entrance to the overboard bypass system arose from the removal of the boundary layer by bypass flow extraction.

At the maximum angle of attack (5.58°, fig. 12(b)) the total pressure pattern was basically a one-per-revolution distortion. The low-pressure regions on the cowl near the bottom and on the centerbody (upper right and left) were regions of flow separation (also shown in fig. 13). On the basis of the gradient in compressor-face total pressure near the wall (fig. 13) separation occurred at cowl rake positions 7, 8, 9, and 12. The separation associated with rakes 7, 8, and 9 arose from operation at large angles of attack. The separation at rake 12 appeared to be a localized condition (see also fig. 9). Separation was also indicated on the hub at rake positions 3 and 11, as noted previously.

The largest total pressure gradients in the radial direction occurred in the lower half of the inlet near midspan. On the basis of relationships governing the generation of turbulence, this region of large total pressure or velocity gradients should then be the region of largest turbulence or dynamic distortion. The upper half of the inlet had lower pressure gradients and hence should have had less dynamic activity. The measured turbulence at the compressor face (fig. 14) varied from 1 to 4 percent of the average compressor-face total pressure. The largest dynamic activity occurred at midspan on rake 7, which was located at the bottom of the inlet. Rake 1, which was located at the top of the inlet, showed the lowest turbulence.

The circumferential distortion is presented in reference 10 and shown in figure 15 in terms of the distortion index $K_{d2}$ and the turbulence correcting factor $\Delta P_{rms}/P_2$. This distortion index system was developed specifically for the TF30-P-3 turbofan engine as part of the TF30/F111

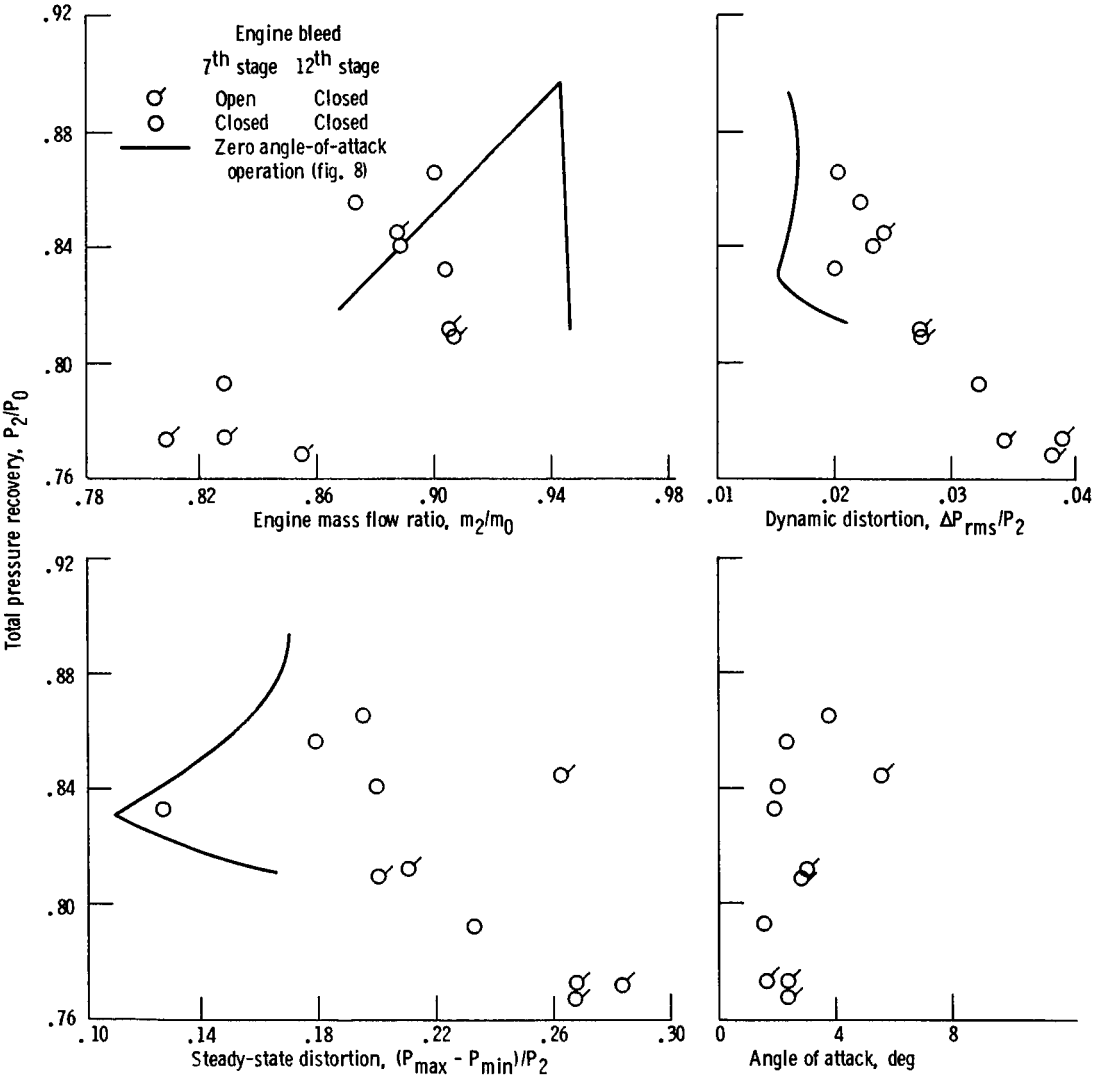


Figure 11.—Inlet performance during incipient surge operation at angle of attack.

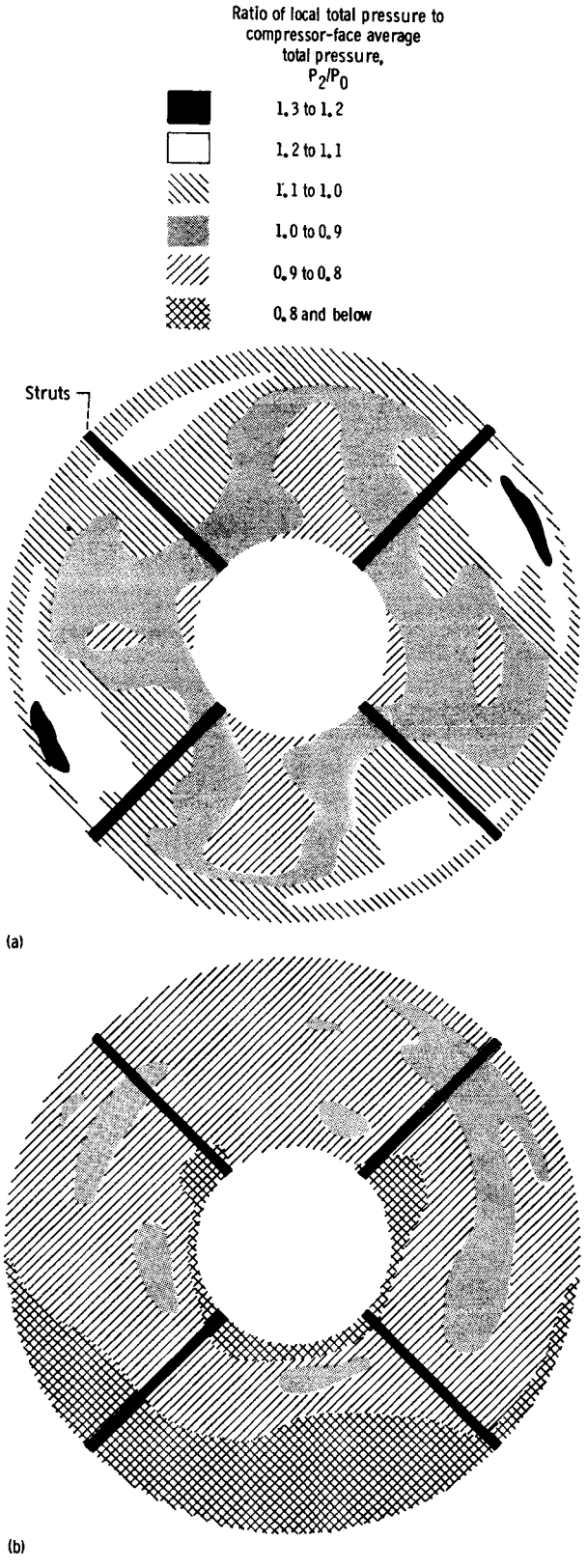


(a) Supercritical operation at zero angle of attack.
(b) Operation at maximum angle of attack.

Figure 12.—Steady-state distortion patterns at compressor face during incipient surge operation, looking downstream.

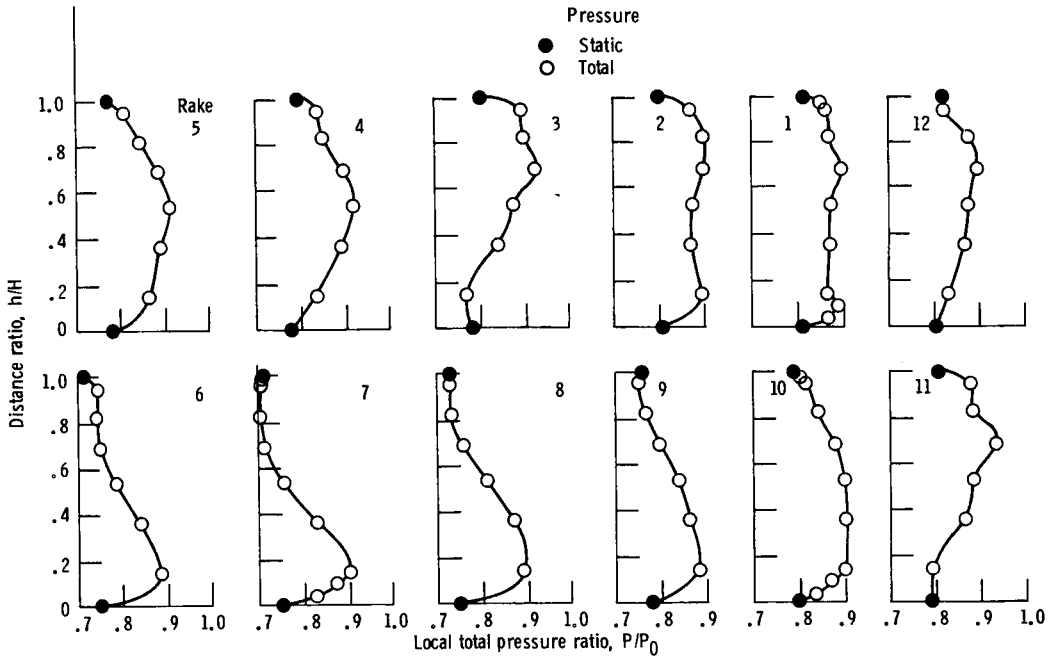


Figure 13.—Radial total pressure profiles at compressor face during operation at maximum angle of attack.

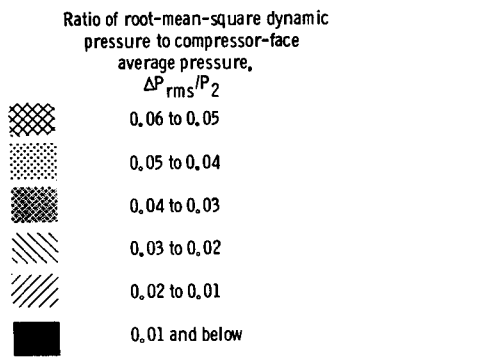


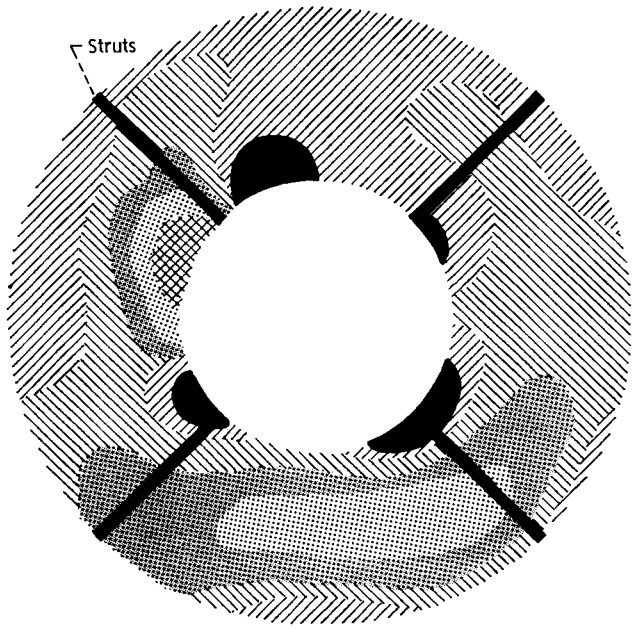


Figure 14.—Dynamic distortion at compressor face during operation at maximum angle of attack, looking downstream.

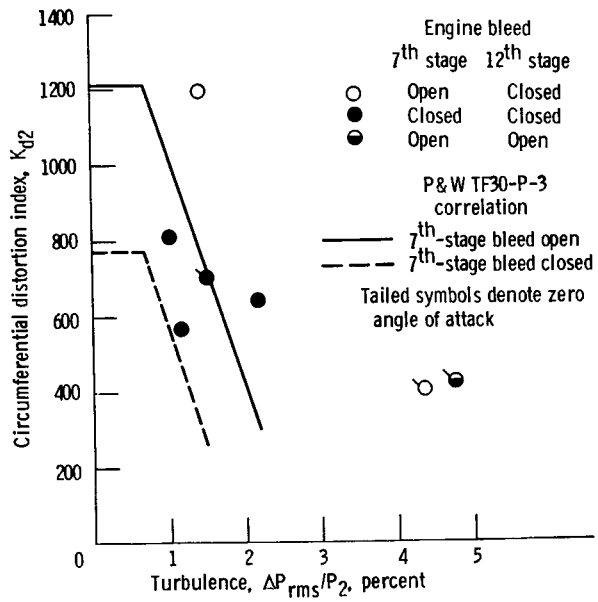


Figure 15.—Application of TF30-P-3 distortion methodology.

program. For a given level of turbulence compressor surge would be predicted whenever the distortion index exceeded the Pratt & Whitney stability limit correlation (fig. 15). As discussed in reference 10, these correlations depend on the flow rate through the engine. The correlations and the data presented in figure 15 are for a corrected flow rate of 66 to 68 kg/s (145 to 150 lb/s). The stability limit correlations were derived from cell testing of the engine behind a turbulence generator and a distortion valve. The distortion patterns considered in the development of the correlation were mainly one per revolution.

The data presented in figure 15 consist of distortion levels based on measurements from the 72 steady-state total pressure probes and of turbulence levels based on measurements from the 36 high-response probes. The dynamic data were filtered with a low-pass filter to 150 Hz for consistency with the stability limit correlations. The analysis of these data presented in reference 10 concluded that agreement between the correlation and the data for no bleed was reasonable at low turbulence levels but not as good at higher turbulence levels.

The engine displayed greater tolerance to distortion when the seventh-stage bleed was open than would be predicted from experience (fig. 15). These data also show that opening the twelfth-stage bleed had little effect on the engine's tolerance to distortion. This is consistent with Pratt & Whitney's experience (ref. 10).

Several differences were noted in the study of reference 10 between the subject data and that upon which the correlation was based. As noted, the distortions encountered in the present study contained four-per-revolution patterns, but the Pratt & Whitney experience on which the correlations were based was for one-per-revolution distortion patterns. The measured turbulence levels were also higher at high frequencies than those used in developing the distortion indices and the turbulence methodology. King et al. (ref. 10) suspect this difference to be related to greater than normal tolerance to turbulence. The level of circumferential distortion in terms of $K_{d2}$ associated with incipient surge (fig. 16) generally increased as the angle of attack was increased. At the maximum attainable angle of attack (5.58°) $K_{d2}$ was 1252. At zero angle of attack $K_{d2}$ varied from 391 to 704, depending on the engine bleed configuration. As mentioned, opening the compressor bleeds made the inlet-engine combination more tolerant of distortion. (Distortion in terms of $K_{d2}$ is also discussed in ref. 10.)

The propulsion system was sensitive to distortions other than circumferential. The magnitudes of radial and dynamic distortions are also important. The inlet-engine tolerated substantially more circumferential distortion in the absence of radial distortion (fig. 17). Opening the compressor bleeds made the inlet-engine more stable. (The dynamic distortion experienced by the propulsion system is described in ref. 10.)

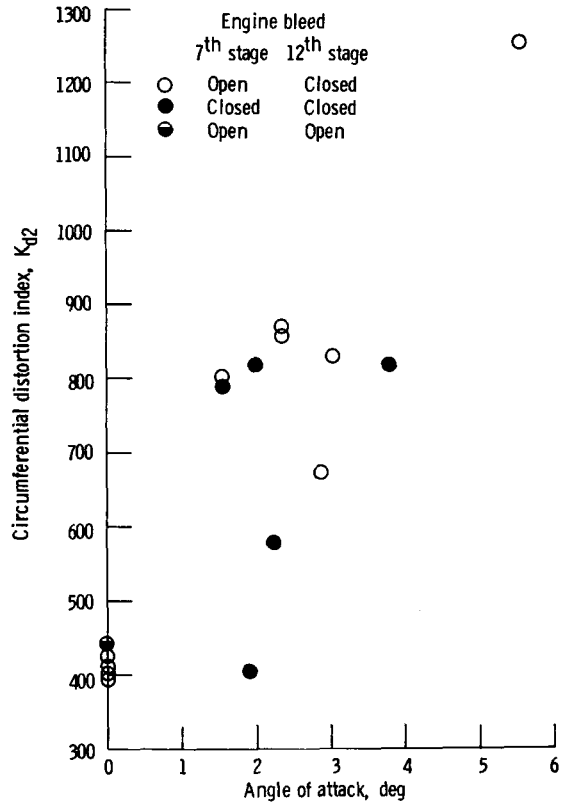


Figure 16.—Circumferential distortion at compressor face with angle of attack.

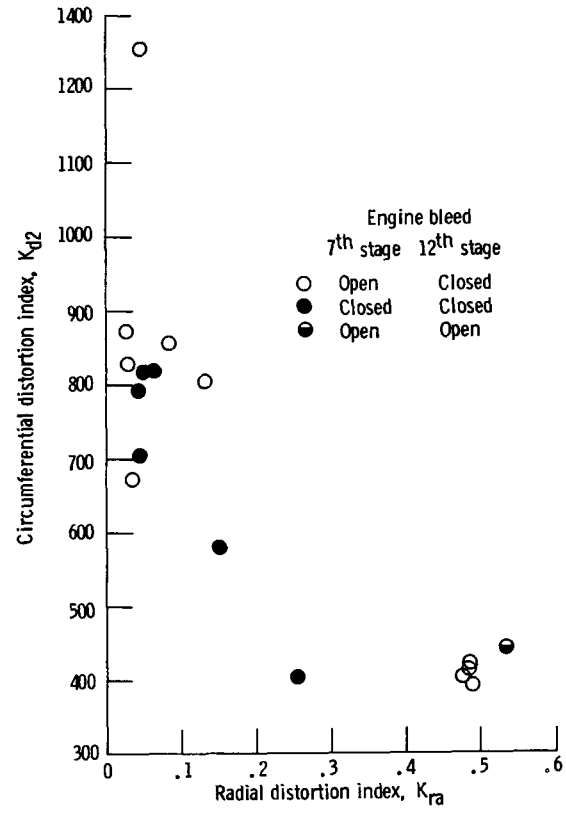


Figure 17.—Circumferential and radial distortion during incipient surge operation at angle of attack.

## Summary of Results

A full-scale, low-bleed, mixed-compression, axisymmetric inlet coupled to a TF30-P-3 turbofan engine was tested to investigate steady-state performance, integrated control system techniques, and inlet-engine compatibility at a free-stream Mach number of 2.5. The inlet had minimum internal contraction, as is consistent with high total pressure recovery and low cowl drag. The following results were obtained:

1. The inlet-engine combination displayed good performance without large quantities of inlet performance bleed. At the match inlet-engine operating condition the inlet pressure recovery was 0.895 at a diffuser throat-exit mass flow ratio of 0.977. The circumferential distortion index $K_{d2}$ was 282; the turbulence correcting factor $\Delta P_{rms}/P_2$ was 0.016.

2. The inlet-engine combination had large-angle-of-attack capability with sustained operation. The maximum angle of attack was limited by engine stall to 5.58°. The steady-state pressure recovery at this angle of attack was 0.845.

3. The inlet-engine combination displayed a high tolerance to generated inlet distortion. At zero angle of attack the total pressure distortion at the compressor face was a four-per-revolution pattern superimposed on a radial pattern. This pattern resulted from the extremely supercritical terminal shock position necessary to create a combined dynamic and steady-state distortion sufficient to induce surge. As the angle of attack was enlarged, the patterns tended toward one-per-revolution steady-state distortion. The surges at large angle of attack were characterized by high circumferential distortion index $K_{d2}$ and low rms levels of turbulence.

Lewis Research Center
National Aeronautics and Space Administration
Cleveland, Ohio, February 19, 1985

# Appendix—TF30-P-3 Distortion Indices

The circumferential distortion index $K_{d2}$ is defined as

$$K_{d2} = \frac{\sum_{i=1}^{6} \left(\frac{\Delta P}{P_{av}}\right)_{2i} \theta_i \left(\frac{1}{D_{ring}}\right)}{\sum_{i=1}^{6} \frac{1}{D_{ring}}}$$

where

$$\left(\frac{\Delta P}{P_{av}}\right)_{2i} = \frac{P_{ring,av} - P_{ring,min}}{P_{ring,\,av}}$$

$i$ is the number of rings (which is equal to the number of radial probes per rake), $\theta_i$ is the largest "arc" of pressure below the rake average in radians, and $D_{ring}$ is the diameter of the ring.

The radial distortion index is defined as

$$K_{ra} = \frac{\sum_{i=1}^{6} \frac{\Delta P}{Q} \left(\frac{1}{D_{ring}}\right)^{2.8}}{\sum_{i=1}^{6} \left(\frac{1}{D_{ring}}\right)^{2.8}}$$

where $Q$ is compressor face dynamic pressure and

$$\Delta P = P_{av} - P_{i,av}$$

and if negative, is set to zero; $P_{av}$ is the average compressor face pressure; $P_{i,av}$ is the local ring average of $P_i$, the local compressor face total pressure on the $i^{th}$ ring.

# References


1. Coltrin, Robert E.; and Choby, David A.: Steady-State Interactions from Mach 1.98 to 2.58 Between a Turbojet Engine and an Axisymmetric Inlet with 60-Percent Internal Area Contraction. NASA TM X-1780, 1969.
2. Cole, Gary L.; Neiner, George H.; and Wallhagen, Robert E.: Coupled Supersonic Inlet-Engine Control Using Overboard Bypass Doors and Engine Speed to Control Normal Shock Position. NASA TN D-6019, 1970.
3. Neiner, George H.; Crosby, Michael J.; and Cole, Gary L.: Experimental and Analytical Investigation of Fast Normal Shock Position Controls for a Mach 2.5 Mixed-Compression Inlet. NASA TN D-6382, 1971.
4. Calogeras, James E.: Experimental Investigation of Dynamic Distortion in a Mach 2.50 Inlet with 60 Percent Internal Contraction and Its Effect on Turbojet Stall Margin. NASA TM X-1842, 1969.
5. Wasserbauer, Joseph F.; Shaw, Robert J.; and Neumann, Harvey E.: Design of a Very-Low-Bleed Mach 2.5 Mixed-Compression Inlet with 45 Percent Internal Contraction. NASA TM X-3135, 1975.
6. Batterton, Peter G.; Arpasi, Dale J.; and Baumbick, Robert J.: Digital Integrated Control of a Mach 2.5 Mixed-Compression Supersonic Inlet and Augmented Mixed-Flow Turbofan Engine. NASA TM X-3075, 1974
7. Baumbick, Robert J.; Batterton, Peter G.; and Daniele, Carl J.: Terminal-Shock and Restart Control of a Mach 2.5 Mixed-Compression Inlet Coupled to a Turbofan Engine. NASA TM X-3104, 1974.
8. Baumbick, Robert J.; Batterton, Peter G.; and Daniele, Carl J.: Effect of Afterburner Lights and Inlet Unstarts on a Mixed-Compression-Inlet Turbofan Engine Operating at Mach 2.5. NASA TM X-3223, 1975.
9. Costakis, William G.: Experimental Investigation of a Simple Distortion Index Utilizing Steady-State and Dynamic Distortions in a Mach 2.5 Mixed-Compression Inlet and Turbofan Engine. NASA TM X-3169, 1975.
10. King, R.W.; Schuerman, J.A.; and Muller, R.G.: Analysis of Distortion Data from TF30-P-3 Mixed Compression Inlet Test. NASA CR-2686, 1976.
11. Braithwaite, Willis M.: Experimental Evaluation of a TF30-P-3 Turbofan Engine in an Altitude Facility: Effect of Steady-State Temperature Distortion. NASA TM X-2921, 1973.

| 1. Report No. | 2. Government Accession No. | 3. Recipient's Catalog No. |
|---|---|---|
| NASA TP-2461 | | |

| 4. Title and Subtitle | 5. Report Date |
|---|---|
| Performance and Surge Limits of a TF30-P-3 Turbofan Engine/Axisymmetric Mixed-Compression Inlet Propulsion System at Mach 2.5 | May 1985 |
| | 6. Performing Organization Code: 505-43-52 |

| 7. Author(s) | 8. Performing Organization Report No. |
|---|---|
| Joseph F. Wasserbauer, Harvey E. Neumann, and Robert J. Shaw | E-2412 |
| | 10. Work Unit No. |

| 9. Performing Organization Name and Address | 11. Contract or Grant No. |
|---|---|
| National Aeronautics and Space Administration<br>Lewis Research Center<br>Cleveland, Ohio 44135 | |
| | 13. Type of Report and Period Covered: Technical Paper |

| 12. Sponsoring Agency Name and Address | 14. Sponsoring Agency Code |
|---|---|
| National Aeronautics and Space Administration<br>Washington, D.C. 20546 | |

15. Supplementary Notes

16. Abstract

Steady-state performance and inlet-engine compatibility were investigated with a low-bleed inlet. The inlet had minimum internal contraction, consistent with high total pressure recovery and low cowl drag. The inlet-engine combination displayed good performance with only about 2 percent of inlet performance bleed. The inlet-engine combination had 5.58° angle-of-attack capability with 6 percent bleed.

| 17. Key Words (Suggested by Author(s)) | 18. Distribution Statement |
|---|---|
| Inlets (supersonic); Propulsion systems; Inlet controls; Inlet distortion | Unclassified - Unlimited<br>STAR Category 07 |

| 19. Security Classif. (of this report) | 20. Security Classif. (of this page) | 21. No. of pages | 22. Price |
|---|---|---|---|
| Unclassified | Unclassified | 20 | A02 |

For sale by the National Technical Information Service, Springfield, Virginia 22161 NASA-Langley, 1985